ELSEVIER

Contents lists available at ScienceDirect

# Journal of Membrane Science

journal homepage: www.elsevier.com/locate/memsci





# Direct, efficient and selective capture of low concentration of CO<sub>2</sub> from natural gas flue gas using a high temperature tubular carbon capture membrane

Shichen Sun, Aidan Billings, Kangkang Zhang, Kevin Huang

Department of Mechanical Engineering, University of South Carolina, Columbia, SC, 29212, USA

#### ARTICLE INFO

Keywords:
Membrane
CO<sub>2</sub> flux
CO<sub>2</sub> purity
CO<sub>2</sub> capturing rate
H<sub>2</sub>O enhancement

#### ABSTRACT

Natural gas (NG) fired power plants emit low concentration (4–5%) of CO<sub>2</sub>, which presents additional technical and economic challenges to the current benchmark amine absorption technology. The newly emerged high-temperature multiphase membranes operated on molten carbonate (MC) chemistry for CO<sub>2</sub> capture/separation/conversion have been demonstrated with great potential to meet this challenge. In this study, we report on the CO<sub>2</sub> capture performance of such a membrane in tubular geometry from a mockup NG flue gas. The membrane is comprised of a mixture of  $Gd_{0.20}Ce_{0.80}O_{1.95}$  (GDC) and MC, in which GDC forms a porous skeleton to contain MC. We show that the membrane with a dimension of 6.1 mm in outer diameter, 5.1 mm in inner diameter and 5 cm in effective length (resulting in 4 cm² effective surface area) can achieve a CO<sub>2</sub> flux density of 0.46-0.55 mL/min·cm² at 650 °C, capturing 97% pure CO<sub>2</sub> at a rate of 37-42% from 5%CO<sub>2</sub>-N<sub>2</sub> using moistened Ar as the sweep gas. The level of performance demonstrated by this study suites the membrane well for stationary CO<sub>2</sub> capture from NG power plants.

## 1. Introduction

Natural gas (NG) fired power plants have surpassed coal fired power plants and become the #1 source of electricity generation in the U.S. in 2019, producing 1.6 billion MWhs or 40.3% of the national electricity supply (vs. 19.3% for coal-fired power plants) [1]. The widespread use of NG is primarily driven by the availability of low-cost shale gas, high efficiency of natural gas combined cycle (NGCC) technology, and growing concerns on  $CO_2/CH_4$  related global warming. With NG as a cleaner fuel, the  $CO_2$  emissions are  $\sim$ 40% less than burning coals. Additionally, there is no emissions of Hg and chloride, and PM, NO<sub>x</sub>, and  $SO_x$  emissions are all at or below the federal regulatory limits currently in effect for NGCC technology.

Although NGCC power plants emit less  $CO_2$ , the total amount of  $CO_2$  annually released to the atmosphere is still staggering. In 2019 alone, the U.S. released  $\sim 0.9$  billion tons of  $CO_2$  from NGCC power plants to the atmosphere [2]. To control global carbon pollution, this source of  $CO_2$  emissions must be curtailed. The current benchmarks of  $CO_2$ -capture/separation technologies are principally based on reversible chemical/physical sorption processes, using liquid solvents and solid sorbents as  $CO_2$  scrubbers [3–5]. However, the cost and energy penalty to

implement these scrubbing technologies into existing power plants are still too high for practical applications. For example, implementing Shell CONSOLV, a benchmark regeneratable "amine absorption" technology, into a 740 MWe NGCC power plant would lower the plant's net efficiency from 53.6% to 47.7% at 90%  $\rm CO_2$  capture capacity and incur a 64% (from \$43.3/MWh to \$70.9/MWh, excluding T&S) hike in LCOE over the baseline case [6]. Therefore, to achieve flue gas carbon capture at a large commercial scale, new transformational carbon capture technologies with lower cost and energy consumption are highly desirable.

Unlike solvent- and sorbent-based  $CO_2$  capture techniques, membrane-based  $CO_2$  capture processes present fundamental advantages in cost and energy consumption due to their capability of delivering high-pressure  $CO_2$ , promoting CO shifting reactions, and not using energy-intensive steam or chemical loads [7–17]. However, the major issues with these size-exclusion and solubility-diffusivity based membranes are the tradeoff between selectivity and permeability, aka. the Robeson upper bound rule. Therefore, developing alternative new membrane technologies to capture  $CO_2$  more selectively and efficiently is greatly needed.

An emerging class of carbon capture membranes, in recent years, are

E-mail address: huang46@cec.sc.edu (K. Huang).

<sup>\*</sup> Corresponding author.

the multiphase solid/molten carbonate (MC) composites [18–24]. This family of carbon transport membranes (CTMs) operates on high-temperature chemistries of ions, or mixed ion/electron transports, without the limitation of Robeson rule [25,26]. Initial laboratory results have shown the great potential of CTMs with high CO $_2$  flux and selectivity in 600–900 °C [18,20,21,27,28]. The operating temperature of these CTMs also matches well with that of the flue-gas at the exit of gas turbine cycle in a NGCC, thus allowing the heat in the flue-gas to be directly utilized for membrane operation. By design, the membrane reactor can be practically inserted between the gas turbines and the heat recovery steam generators (HRSG) to directly capture hot CO $_2$ , without changing the flue gas temperature (~650 °C) for the downstream HRSG and steam turbine cycle, thus potentially saving energy and cost.

In this study, we show that a promising tubular ceramic  $(Gd_{0.20}Ce_{0.80}O_{1.95} \ (GDC))$ -molten carbonate (MC) dual-phase membrane can efficiently and selectively capture 5%  $CO_2$  from a mockup natural gas flue gas at 650 °C. Compared to conventional disk-type CTM membranes, tubular membranes have advantages in  $CO_2$  capture efficiency (less bypass), easy gas sealing, and tolerance to stresses [29–33]. We particularly emphasize the beneficial effect of steam on the  $CO_2$  flux density and capture efficiency, given the fact that there is easy access to steam in NGCC power plants.

## 2. Experimental procedure

#### 2.1. Preparation of GDC-MC dual phase tubular membrane

The GDC porous tubular membrane was fabricated via a coldisostatic press (CIP) method. Briefly,  $Gd_{0.20}Ce_{0.80}O_{1.95}$  (GDC-20 M, Fuelcellmaterials) powder was first intimately mixed with carbon black as a pore former, with a volume ratio of 1:1, in ethanol by ball-milling for 24 h. After mixing and drying, the powder mixture was densely packed into a rubber mold, with a stainless-steel rod as insert, and a flat cap sealed on top. The powder mixture was then pressed under 150 MPa for 30 min in a CIP. After pressing, the tube was removed from the mold and slightly polished on its surface with sandpaper. It was then sintered at 600 °C for 2 h in air, to remove the carbon pore former, and then 1200 °C for 5 h to achieve good mechanical strength.

MC infiltration for the GDC tubular membrane was carried out exsitu. First, the open end of the GDC tubular membrane was tied to a platinum string, and a porous alumina cylinder was inserted to adsorb any MC that flowed into the membrane, preventing the formation of a detrimental MC overlayer. The tubular membrane assembly was then heated to 550 °C at 1 °C/min in a furnace, hanging above a crucible filled with a eutectic mixture of Li<sub>2</sub>CO<sub>3</sub> ( $\geq$ 99%, Alfa Aesar) and Na<sub>2</sub>CO<sub>3</sub> ( $\geq$ 99%, Alfa Aesar) in a molar ratio of 52:48. Upon reaching 550 °C, the membrane was slowly dropped into the MC, with the closed-end facing down, and then kept for 30 min. After that, the membrane was slowly pulled up from the MC, and the porous alumina tube was removed from the membrane, followed by cooling to room temperature at 1 °C/min. After infiltration, both sides of the tubular membrane were gently polished with sandpaper to remove the residual carbonate overlayer.

## 2.2. Characterization of membranes

The phase structures of GDC tubular membrane after sintering and infiltration were examined with X-ray diffraction (XRD, Rigaku D/MAX-2100) with Cu K $\alpha$  radiation ( $\lambda=1.5418$  Å) from 20°-80°. Relative densities ( $\epsilon$ ) of the sintered porous GDC tubes were determined by the Archimedes' method. To obtain other microstructure measurements of the porous matrix, e.g. tortuosity ( $\tau$ ) and average pore radius (r), we used a helium permeation method as described in previous works [34, 35]. Briefly, a porous GDC tube was first sealed to a stainless-steel sample holder with a silicone paste, which was then inserted into a chamber connected to a helium cylinder and a mass flow controller. The downstream pressure ( $P_L$ ) of the membrane was varied via an outlet

valve, while the pressure difference across the membrane ( $\Delta P$ ), the inlet pressure of the membrane ( $P_I$ ), and the flow rate (f) are simultaneously recorded with a pressure differential gauge, pressure gauge, and bubble flow meter, respectively.

The permeance of helium, F, through the porous matrix is calculated by

$$F = \left(\frac{Q}{S \cdot (P_I - P_L)}\right) \tag{1}$$

where S is the active area for the permeating gas and Q is the molar flow rate of permeating helium calculated from the bubble flow meter.

According to Darcy's law, F is given by

$$F = \alpha + \beta \cdot \left( P_I - \frac{\Delta P}{2} \right) \tag{2}$$

where  $\alpha$  and  $\beta$  are permeability coefficients related to Knudsen flow and viscous flow, respectively. The pore radius, r, is then calculated by

$$r = 8.4818\mu\sqrt{\frac{RT}{M_w}} \left(\frac{\beta}{\alpha}\right) \tag{3}$$

where R is the gas constant, T is absolute temperature, and  $M_w$  is the molecular weight of helium. Since  $\alpha$  and  $\beta$  are related to  $\epsilon/\tau$  by the following equations

$$\alpha = 1.06 \left(\frac{\varepsilon}{\tau}\right) \left(\frac{r}{L\sqrt{RTM_w}}\right) \tag{4}$$

$$b = 0.125 \binom{\varepsilon}{\tau} \left( \frac{r^2}{L\mu RT} \right) \tag{5}$$

where L is the thickness of the porous matrix and  $\mu$  is the viscosity of helium,  $\tau$  can be further calculated from the known porosity ( $\epsilon$ ) and r values.

The microstructure of the GDC-MC tubular membranes after sintering, infiltration, and tests were carefully examined by a field emission scanning electron microscope (FESEM, Zeiss GeminiSEM 500) and energy dispersive spectroscopy (EDS, AMETEK, EDAX ELECT SUPER) at an accelerating voltage of 5 kV and an acquisition time of 300 s, and the phase purity of GDC-MC tubular membranes after tests were analyzed by same X-ray diffraction (XRD, Rigaku D/MAX-2100) under the same condition as described above.

## 2.3. Tubular membrane assembly

We used a homemade fixture for membrane performance testing in capturing/separating CO<sub>2</sub>; the setup is schematically shown in Fig. 1. To assemble the test article, the one-end closed tubular membrane was first mounted and sealed onto an alumina supporting tube with silver paste, followed by curing at 150  $^{\circ}\text{C}$  for 2 h. The sealed tubular membrane was then placed horizontally inside a quartz tube with flanges on both ends in a tubular furnace. The outer surface of the tubular membrane, or the permeate surface, was fed with the sweep gas Ar, and the inner surface, or the retentate surface, was fed with CO2-N2 mixture. To avoid gas bypass, the free volume inside the quartz tube was occupied by thermal blocks (insulation materials) wrapped with ceramic wool, forcing Ar to flow over the outer surface of the membrane. The sweep Ar was also moistened by a humidifier and the water content in Ar was measured online by a humidity sensor (Vaisala model 332). The composition of sweep effluent was analyzed by a micro-GC (Agilent MicroGC-490). The same humidity sensor was also switchable to the feed gas line for detecting water content transported though the transmembrane.

## 2.4. CO<sub>2</sub> flux measurements

To examine the effect of the partial pressure of steam (pH2O) on the

Fig. 1. Schematic of GDC-MC tubular membrane testing setup.

 $\rm CO_2$  flux, a range of steam contents (0–15%) were generated by passing the Ar permeate gas through a homemade water saturator at different temperatures before the gas was fed to the outside of the tube. Simultaneously, a simulated flue gas mixture of 95%N<sub>2</sub>/5%CO<sub>2</sub> at a flow rate of 100 mL/min was fed to the inner surface of the membrane as the retentate gas. The real steam contents in the carrier gas and in the retentate exhaust were determined by the on-line humidity sensor.

To examine the effect of the partial pressure of  $CO_2$  ( $pCO_2$ ) in the retentate gas on the  $CO_2$  flux, the  $CO_2$  concentration in  $N_2$  was varied between 5, 15, and 50%, with a fixed total flow rate of 100 mL/min. The permeate gas for this study was Ar at a flow rate of 100 mL/min saturated with  $3\%H_2O$ .

Finally, to examine the short-term stability of the membrane under different flow rate conditions, we used 80, 100, and 150 mL/min Ar flows saturated with  $3\%H_2O$ , while keeping the total flow rate on the retentate side the same to avoid possible influence from pressure difference, i.e, 80/100/150 mL/min, with a fixed composition of  $95\%N_2/5\%CO_2$ .

In all flux measurement tests, the temperature was fixed at 650  $^{\circ}\text{C}$ . The composition of the permeate side effluent was analyzed by an online gas chromatographer (Micro-GC 490, Agilent). At each condition (pH<sub>2</sub>O/pCO<sub>2</sub>/flow rate), 1 h was given to ensure full stability before data was taken. The final CO<sub>2</sub> and N<sub>2</sub> flux densities (as an indicator of leakage) permeated through the membrane were calculated using the following equations:

$$J_{CO_2} = \frac{C_{CO_2} - C_{Leak}}{1 - C_{CO_2} - C_{N_2}} \times \frac{F_{Ar}}{A}$$
 (6)

$$J_{N_2} = \frac{C_{N_2}}{1 - C_{CO_2} - C_{N_2}} \times \frac{F_{Ar}}{A} \tag{7}$$

where  $F_{Ar}$  is the flow rate of the Ar permeate gas, A is the effective area of the membrane,  $C_{CO_2}$  and  $C_{N_2}$  is the measured concentration of  $CO_2$  and  $N_2$  in permeate exhaust, respectively. To correct for the leakage through the membrane, the  $CO_2$  flux was corrected by subtracting  $C_{Leak}$ , which equals  $C_{N_2} * \left(\frac{pCO_2}{1-pCO_2}\right)$ .

The  ${\rm CO_2}$  capture rate (CCR) was also calculated via the following equation:

$$CCR = \frac{C_{CO_2} - C_{Leak}}{p_{CO_2} * F_{feed}} \times \frac{F_{Ar}}{A} \times \frac{1}{1 - C_{CO_2} - C_{N_2}}$$
(8)

where  $p_{CO2}$  and  $F_{feed}$  are the partial pressure of  $CO_2$  and the flow rate of the retentate gas mixture, respectively.

In addition, the water flux through the membrane, from the permeate side to retentate side, was also calculated:

$$J_{H_{20}} = \frac{C_{H_{20}} * F_{feed}}{A} \tag{9}$$

where  $C_{H_2O}$  is the concentration of  $H_2O$  in the retentate side effluent, analyzed by a humidity sensor.

### 3. Results and discussions

#### 3.1. Tubular membrane

The physical image of the fabricated tubular membrane with one end closed is shown in Fig. 2 at different states. The final dimension of the sintered tubular membrane is 48 mm in length, 6.1 mm in outer diameter, and 5.1 mm in inner diameter. After assembling the tube membrane on a supporting  $\rm Al_2O_3$  tube with silver sealant, the resulting effective surface area is 4.0 cm².

Fig. 3 shows the XRD patterns of GDC tubular membrane after sintering at 1200 °C, after infiltration with MC and after testing. The GDC-20 ( $Ce_{0.8}Gd_{0.2}O_{2.x}$ ) peaks are well maintained after sintering and MC infiltration, while only trace amount of LiNaCO<sub>3</sub> is detected in the crushed GDC-MC tubular membrane after testing. These observations suggest good chemical stability of GDC during the processing and testing process and good compatibility with MC. The porosity ( $\epsilon$ ), tortuosity ( $\tau$ ) and average pore diameter determined by Archimedes' method and helium permeation method are 30%, 1.94 and 0.27  $\mu$ m, respectively.

Fig. 4(a) shows the cross section of the membrane at lower magnification, indicating the thickness of the membrane is  $\sim\!0.5$  mm. At higher magnification, Fig. 4(b) shows that the membrane possesses a porous structure, with uniformly distributed pores at a pore size of  $<\!1$   $\mu m$  after sintering at 1200 °C for 5 h, which is consistent with the results obtained from helium permeation method. After infiltration of MC into the porous GDC skeleton, Fig. 4(c) shows a dense microstructure with the pores in the GDC-MC skeleton filled with MC. It is worth mentioning that an obvious overlayer of carbonates can be seen in Fig. 4(d) on some part of the inner surface of the membrane, which indicates that the inserted porous alumina cylinder did not fully absorb all overflowed MC. Therefore, it is necessary to carry out additional cleaning to remove the

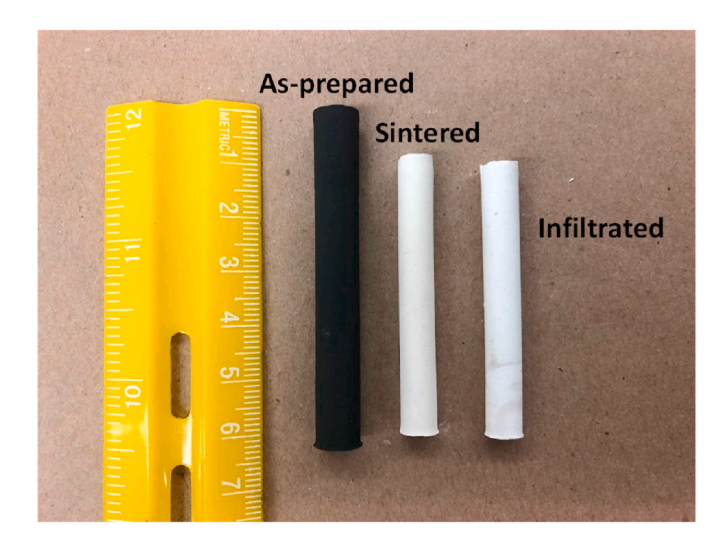


**Fig. 2.** Picture of tubular membranes in the state of as-pressed, as-sintered, and after-infiltration from left to right, respectively.

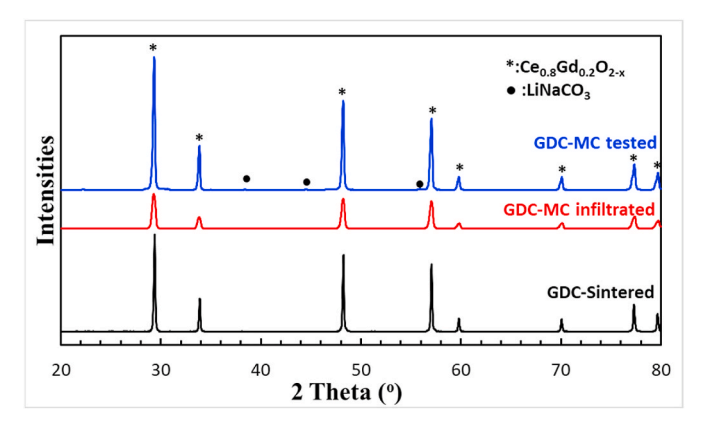


Fig. 3. XRD patterns of GDC tubular membrane after sintering, infiltration, and testing.

excess surface overlayer. We typically used warm water to wipe the membrane surfaces before flux testing. It is worth mentioning that such MC overlayer can also be minimized by controlling the infiltration time

as demonstrated in the work [30].

## 3.2. The effect of pH<sub>2</sub>O in permeate gas on $J_{CO2}$

The effect of pH $_2$ O on the J $_{CO2}$  of the GDC-MC tubular membrane was studied at 650 °C and the results are shown in Fig. 5. With 5% CO $_2$ –N $_2$  as the retentate gas and dry Ar as permeate gas, J $_{CO2}$  stabilizes at  $\sim$ 0.35 mL/min·cm $^2$  with a CCR of  $\sim$ 28%. Such J $_{CO2}$  is in agreement with the calculated 0.378 mL/min·cm $^2$  by equation below [36].

$$J_{CO_2} = -\left(\frac{\varepsilon}{\tau}\right) \frac{RT}{4F^2 L} \frac{\varphi \sigma_c (1-\varphi)\sigma_O}{\varphi \sigma_c + (1-\varphi)\sigma_O} \ln \frac{P''_{CO_2}}{P'_{CO_2}}$$
(10)

where  $\epsilon$  and  $\tau$  are the porosity and the tortuosity of the porous GDC, respectively; R is the gas constant; T is the absolute temperature in K; F is Faraday's constant; L is the thickness of the membrane,  $\sim$ 0.05 cm;  $\phi$  is the volume fraction of the MC phase;  $\sigma_c$  and  $\sigma_o$  are the conductivities of carbonate-ions and oxide-ions in S/cm, respectively;  $P_{CO_2}^{'}$  and  $P_{CO_2}^{''}$  are the partial pressures at the feed and permeate sides in Pa, respectively.

With  $pH_2O=0.03$  atm in Ar permeate gas, both  $J_{CO2}$  and CCR increase to  $\sim 0.45$  mL/min·cm<sup>2</sup> and  $\sim 36\%$ , respectively. With a further

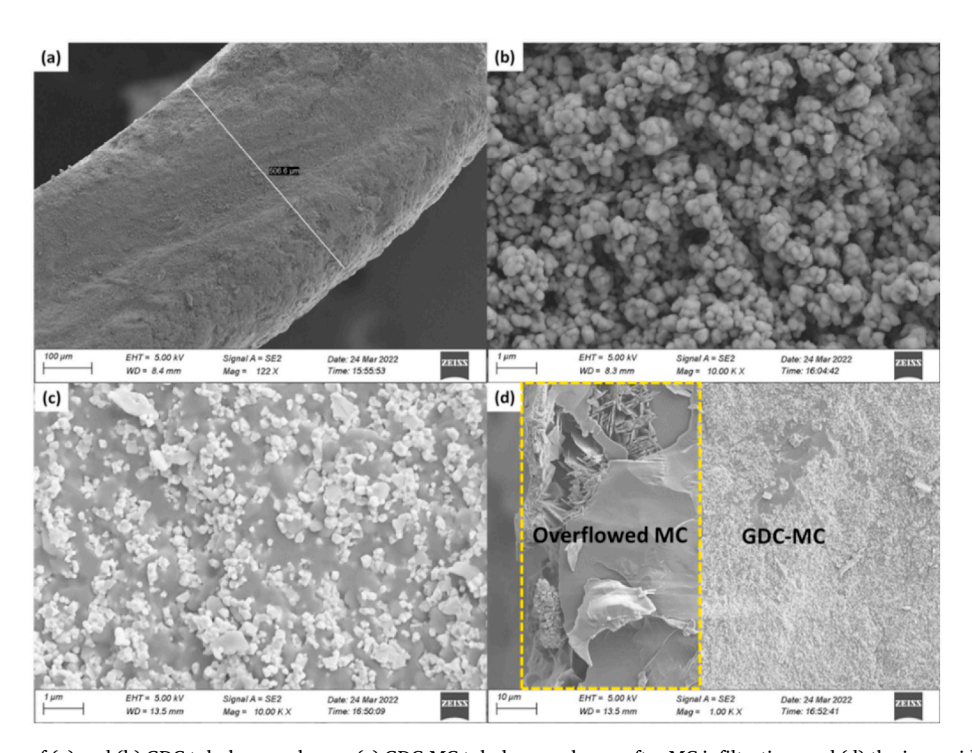


Fig. 4. Cross-section image of (a) and (b) GDC tubular membrane, (c) GDC-MC tubular membrane after MC infiltration, and (d) the inner side of GDC-MC membrane after infiltration (The excess MC is indicated within the dashed line).

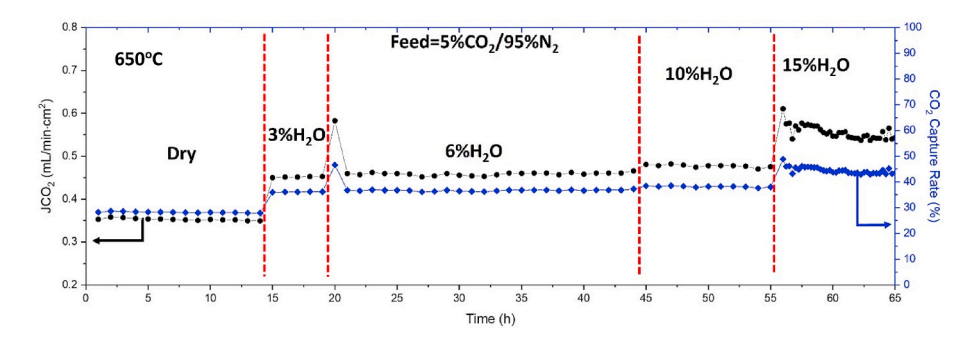


Fig. 5.  $J_{CO2}$  and CCR of a GDC-MC tubular membrane measured at 650 °C and various  $pH_2O=0$ , 0.03, 0.06, 0.1 and 0.15 atm with  $5\%CO_2$ – $N_2$  as the retentate gas mixture.

increase in pH $_2$ O to 0.06, 0.10 and 0.15 atm, both J $_{CO2}$  and CCR increase to  $\sim$ 0.46,  $\sim$ 0.48,  $\sim$ 0.55 mL/min·cm $^2$ , and  $\sim$ 37,  $\sim$ 38,  $\sim$ 42%, respectively. A low N $_2$  leakage at the level of  $\sim$ 0.01 mL/min·cm $^2$  was found in both dry and wet conditions, giving a high CO $_2$  purity of  $\sim$ 97% during the capture process. It is noted that J $_{CO2}$  remains rather stable until pH $_2$ O increases to 15%, when some fluctuations are observed. We speculate that the change in flux upon switching to higher H $_2$ O content may represent the establishment of the equilibrium between H $_2$ O and MC.

We have previously explained the H2O-enhanced CO2 flux phenomenon by a CO<sub>2</sub>/H<sub>2</sub>O co-transport mechanism [37]. In this mechanism, the reaction between H<sub>2</sub>O and CO<sub>3</sub><sup>2-</sup> produces OH<sup>-</sup>; the latter moves in opposite direction of  $CO_3^{2-}$  in the MC phase, i.e. from the permeate side toward the retentate side, charge balancing  $CO_3^{2-}$ . At the retentate side surface,  $OH^-$  reaction with  $CO_2$ , forming  $H_2O$  and  $CO_3^{2-}$ . The counter-diffusion of OH<sup>-</sup> accelerates CO<sub>3</sub><sup>2-</sup>, thus enhancing CO<sub>2</sub> flux. Based on this mechanism, the flux of CO2 at the permeate side should be equal to that of H<sub>2</sub>O at the retentate side. To verify this hypothesis, we measured H<sub>2</sub>O concentration in the effluent of the retentate gas and converted into flux. Fig. 6 compares the measured J<sub>CO2</sub> and J<sub>H2O</sub>. At each H<sub>2</sub>O content at the permeate side, J<sub>CO2</sub> and J<sub>H2O</sub> are comparable within a certain error bar. We speculate that the difference could be originated from H2O content measurement. The humidity sensor typically has a higher uncertainty at higher H2O contents. Nevertheless, the trend is clear, i.e. the higher the H<sub>2</sub>O content in the permeate gas, the higher JH2O at the retentate gas effluent and JCO2 in the permeate gas effluent, respectively.

# 3.2.1. The effect of $pCO_2$ in retentate gas on $J_{CO2}$

The effect of  $p\text{CO}_2$  in the retentate gas on the  $J_{\text{CO}2}$  was also studied at 650 °C. In this study, the Ar permeate gas was constantly saturated with 3%H<sub>2</sub>O. The results are shown in Fig. 7, where  $J_{\text{CO}2}$  and CCR are stabilized at ~0.43 mL/min·cm² and 36% after ~20 h with a 5%CO<sub>2</sub>–N<sub>2</sub> as the retentate gas. At  $p\text{CO}_2=0.15$  and 0.50,  $J_{\text{CO}2}$  increases correspondingly to ~0.71 and ~1.22 mL/min·cm², while CCR decreases significantly to ~18% and ~10%, respectively. The decrease of CCR at higher  $p\text{CO}_2$  suggests that the small tubular membrane in use has limited capability of transporting all CO<sub>2</sub> through the membrane of a definite surface area. To increase the CCR, increasing CO<sub>2</sub> flux density or enlarging tube active area is needed; the latter is, however, a more expensive solution.

The stability test on the membrane was carried out at 650 °C and

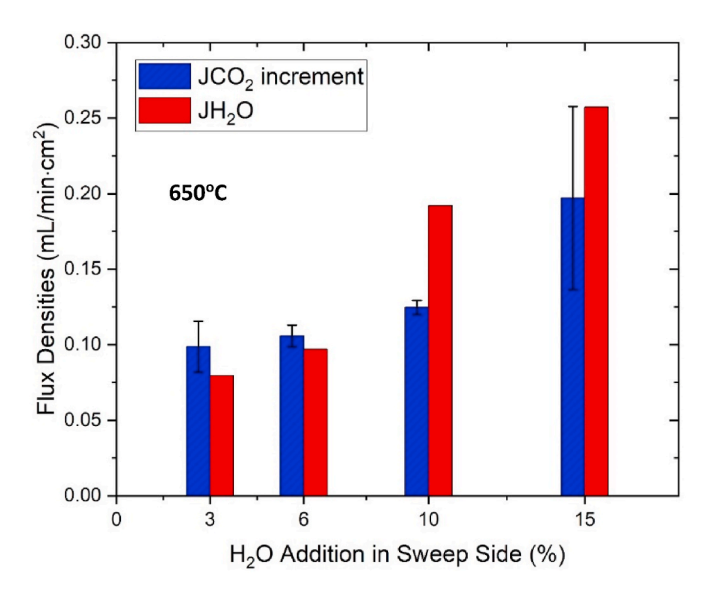
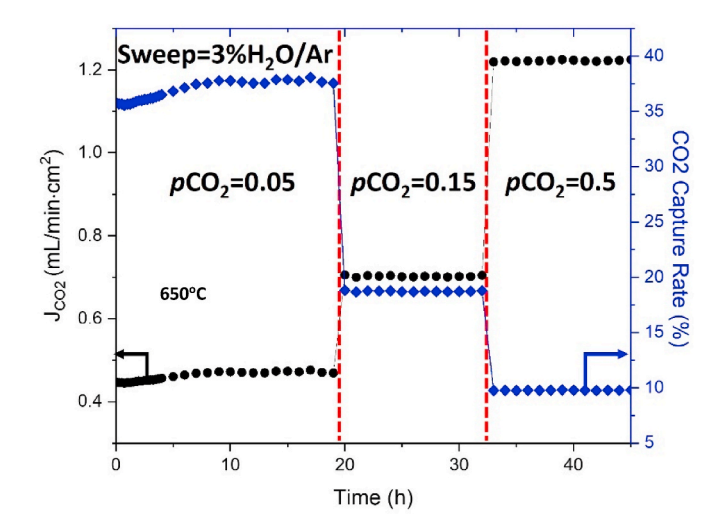


Fig. 6.  $J_{\rm CO2}$  incremental and  $J_{\rm H2O}$  versus  $H_2O$  content measured at 650  $^{\circ}C$  in permeate gas Ar.



**Fig. 7.** (a)  $J_{\rm CO2}$  and  $CO_2$  capture rate of a GDC-MC tubular membrane measured at 650 °C with various  $p{\rm CO}_2=0.05$ , 0.15 and 0.5 with 3%H<sub>2</sub>O/Ar as the permeate gas.

different flow rates; the results are shown in Fig. 8. Despite two obvious changes at the switch of the flow rate, which is likely related to the pressure change induced by flow rate change, no significant difference in  $J_{\rm CO2}$  was found when the total flow rates of both retentate and permeate gases were varied simultaneously from 80 to 100 mL/min, while there was a slight increase in  $J_{\rm CO2}$  (from  $\sim\!0.48$  to  $\sim\!0.51$  mL/min·cm²) as the flow rate was increased to 150 mL/min. This finding suggests the limited capacity of the membrane with a definite surface area to handle high mass flow of CO2-containing stream. This trend is in fact similar to the early finding in Fig. 7 that CCR decreases with CO2 concentrations.

Table 1 compares the results of this work with other tubular membranes of the same chemistry. The GDC-MC tubular membrane of this study, with the largest effective area of 4 cm $^2$  demonstrated, shows the best performance among all tubular CTM membranes, given the lowest  $\rm CO_2$  concentration and intermediate temperature.

## 3.3. Post-test analysis of the membrane

After the stability tests, the surface and internal structures of the membrane were further examined by SEM/EDS. Fig. 9(A) and (B) shows that the interior of the membrane remained dense without significant loss of MC during the test, which supports the stable  $J_{\rm CO2}$  observed.

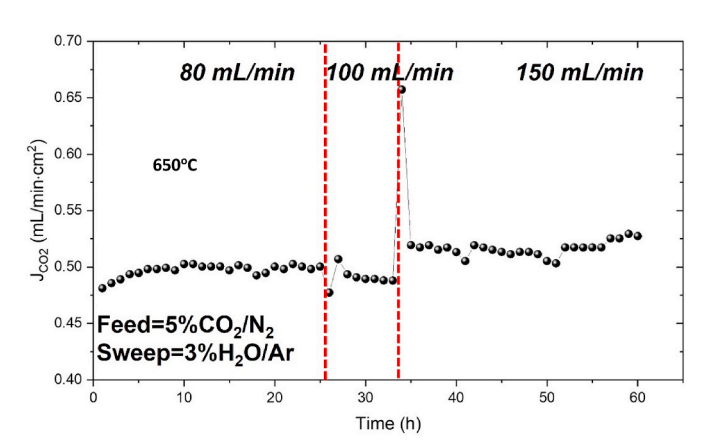


Fig. 8.  $J_{CO2}$  vs. time at different total flow rates on both retentate and permeate sides. Temperature: 650 °C; retentate gas: 5%CO<sub>2</sub>–N<sub>2</sub>; permeate gas: 3%H<sub>2</sub>O–Ar.

Table 1 Comparison of  $CO_2$  permeation performance for different CTM tubular membranes.

Ceramic phase	Thickness (mm)	Area (cm²)	Feed $P_{\rm CO2}$ , atm	T (°C)	$J_{CO2}$ (mL/min·cm <sup>2</sup> )	Ref.
$La_{0.6}Sr_{0.4}Co_{0.8}Fe_{0.2}O_{3-\delta}$ (LSCF)	0.4	2.2	0.5	650-850	0.061-0.13	[38]
Yttria-stabilized zirconia (YSZ)	0.2-0.5	2.2	0.5	500-900	0.082-1.0	[39]
$SrFe_{0.8}Nb_{0.2}O_{3-\delta}$ (SFN)	0.22	0.75	0.5	500-850	0.09-0.64	[40]
$Ce_{0.8}Sm_{0.2}O_{2-\delta}$ (SDC)	0.1-0.15	0.75	0.2	500-700	0.09-1.79	[41]
SDC-SDC/La <sub>2</sub> NiO <sub>4</sub> (LNO)	~0.23	1.32	0.5	550-750	0.36-2.3	[30]
GDC	0.5	4.0	0.05	650	0.35-0.55	This work

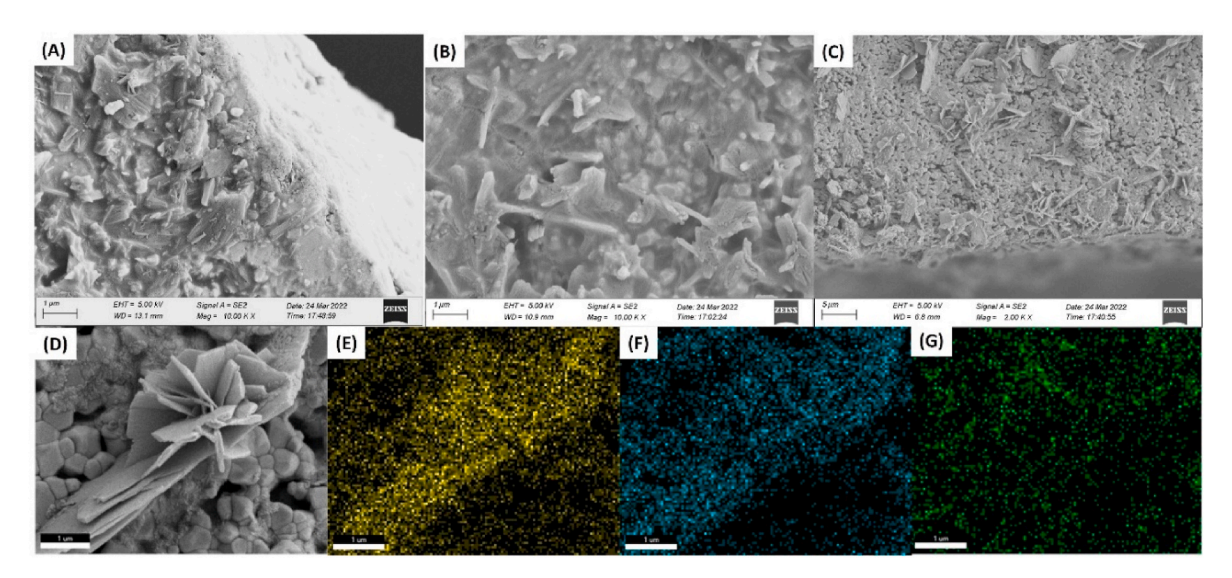


Fig. 9. Cross-sectional views of (A) feed, (B) middle, and (C) permeate side of GDC-MC tubular membrane and (D) close look at flakes by SEM and elemental mapping by EDS: (E) O, (F) C and (G) Na.

However, on the permeate side surface, some flake like materials are found; see Fig. 9(C) and (D). The EDS analysis in Fig. 9(E) and (F) indicates that the flakes are rich in C and O, implying a likely carbonate phase even though EDS cannot detect Li. The fact that the flakes lack Na, as shown in Fig. 9(G), infers that it might be only Li-rich carbonate such as  $\text{Li}_2\text{CO}_3$  and  $\text{Li}_3\text{HCO}_3$ . We have previously observed the same phenomenon [35]. We then conclude that the flake like materials might be the product of hydrated carbonate recrystallized during cooling.

## 4. Conclusions

In this study, a tubular GDC-MC membrane with an active surface area of 4 cm<sup>2</sup> has been successfully fabricated via a CIP method. With 5%CO2-N2 as the retentate gas and dry Ar as the permeate gas, the membrane exhibits  $J_{CO2}=0.35~\text{mL/min}\cdot\text{cm}^2$  and CCR =28% at 650  $^{\circ}\text{C}$ . The J<sub>CO2</sub> and CCR are further enhanced by moistening the permeate Ar gas, reaching 0.45–0.55 mL/min·cm<sup>2</sup> and 37–42%, respectively, at 3-15% H<sub>2</sub>O. The measured H<sub>2</sub>O flux at the retentate side matches, in general, with the measured CO<sub>2</sub> flux at the permeate side, supporting the co-transport mechanism of CO2 and H2O in the MC phase. As CO2 concentration in the retentate gas increases, CO2 flux increases correspondingly, but CCR decreases, implying the limited capability of the membrane of the current geometry (small surface area) to capture high concentration of CO2. With increasing the length and diameter of the membrane, the CO<sub>2</sub> capturing ability (or CCR) is expected to improve. The post-test analysis indicates that the membrane remains dense without sign of MC loss after testing. The flake-like substance on the surface of the permeate side surface are observed, likely an indicator of hydrated products.

#### Author's statement

Shichen Sun: performed experiments, data analysis and manuscript drafting, Aidan Billings: performed powder and tube making, Kangkang Zhang: performed porosity and tortuosity measurements, Kevin Huang: supervising, conceptualization and finalizing manuscript.

# Declaration of competing interest

The authors declare that they have no known competing financial interests or personal relationships that could have appeared to influence the work reported in this paper.

# Data availability

Data will be made available on request.

## Acknowledgement

We would like to thank US Department of Energy, Office of Fossil Energy, National Energy Technology Laboratory (Award # DE-FE-0031634), and National Science Foundation (Award # CBET-1924095) for supporting this work.

## References

- Natural gas generators make up the largest share of overall U.S. generation capacity. https://www.eia.gov/todayinenergy/detail.php?id=34172#, 2020.
- [2] o.C.e.p, How much carbon dioxide is produced per kilowatthour of U.S. electricity generation?. https://www.eia.gov/tools/faqs/faq.php?id=74&t=11#:~:text=In% 202019%2C%20total%20U.S.%20electricity, 2020.
- [3] Y.G. Zhang, J.Y.G. Chan, Sustainable chemistry: imidazolium salts in biomass conversion and CO2 fixation, Energy Environ. Sci. 3 (2010) 408–417.

- [4] S. Smart, C.X.C. Lin, L. Ding, K. Thambimuthu, J.C.D. da Costa, Ceramic membranes for gas processing in coal gasification, Energy Environ. Sci. 3 (2010) 268–278
- [5] Q.A. Wang, J.Z. Luo, Z.Y. Zhong, A. Borgna, CO2 capture by solid adsorbents and their applications: current status and new trends, Energy Environ. Sci. 4 (2011) 42–55.
- [6] A.Z. Robert James, Keairns Dale, Marc Turner, Mark Woods, Norma kuehn, cost and performance baseline for fossil energy plants volume 1: bituminous coal and natural gas to electricity, in: NETL-PUB-22638, 2019.
- [7] w.p. d Shekhawal, in: A Review of Carbon Dioxide Selective Membranes, NETL, 2003.
- [8] T.Y.H. Kawamura, N.N. Balagopal, K. Nakagawa, S. Nakao, Dual-ion conducting lithium zirconate-based membranes for high temperature CO2 separation, J. Chem. Eng. Jpn. 38 (2005) 322–328.
- [9] E.J.G.a.T. O'Brien, Review of novel methods for carbon dioxide separation from flue and fuel gases, Fuel Process. Technol. 86 (2005) 1423–1434.
- [10] N.Y. Du, H.B. Park, M.M. Dal-Cin, M.D. Guiver, Advances in high permeability polymeric membrane materials for CO2 separations, Energy Environ. Sci. 5 (2012) 7306–7322.
- [11] T.F.J.D. Figueroa, S. Plasynski, H. McIlvried, R.D. Srivastava, Advances in CO2 capture technology—The US Department of Energy's carbon sequestration program, Int. J. Greenh. Gas Control 2 (2008) 9–20.
- [12] R. Quinn, J.B. Appleby, G.P. Pez, New facilitated transport membranes for the separation of carbon-dioxide from hydrogen and methane, J. Membr. Sci. 104 (1995) 139–146.
- [13] M.R. Cerón, L.S. Lai, A. Amiri, M. Monte, S. Katta, J.C. Kelly, M.A. Worsley, M. D. Merrill, S. Kim, P.G. Campbell, Surpassing the conventional limitations of CO2 separation membranes with hydroxide/ceramic dual-phase membranes, J. Membr. Sci. 567 (2018) 191–198.
- [14] W. Xing, A. Støre, Contact angle screening and asymmetric dual-phase CO2 separation membranes, J. Membr. Sci. 652 (2022), 120447.
- [15] J. Fabian-Anguiano, M. Ramírez-Moreno, H. Balmori-Ramírez, J. Romero-Serrano, I. Romero-Ibarra, X. Ma, J. Ortiz-Landeros, Syngas production with CO2 utilization through the oxidative reforming of methane in a new cermet-carbonate packed-bed membrane reactor, J. Membr. Sci. 637 (2021), 119607.
- [16] L. Grima, G.A. Mutch, P.B. Oliete, W. Bucheli, R. Merino, E.I. Papaioannou, J. Bailey, M. Kok, D. Brett, P. Shearing, High CO2 permeability in supported molten-salt membranes with highly dense and aligned pores produced by directional solidification, J. Membr. Sci. 630 (2021), 119057.
- [17] M. Starykevich, A. Jamale, K. Yasakau, F. Marques, Novel molten phase route for composite CO2 separation membranes, J. Membr. Sci. (2022), 120806.
- [18] P. Zhang, J. Tong, K. Huang, X. Zhu, W. Yang, The current status of high temperature electrochemistry-based CO2 transport membranes and reactors for direct CO2 capture and conversion, Prog. Energy Combust. Sci. (2021) 82.
- [19] J.H.P.S.J. Chung, D. Li, J.-I. Ida, I. Kumakiri, Jerry Y.S. Lin, Dual-phase metalcarbonate membrane for high-temperature carbon dioxide separation, Ind. Eng. Chem. Res. 44 (2005) 7999.
- [20] L. Zhang, N. Xu, X. Li, S. Wang, K. Huang, W.H. Harris, W.K.S. Chiu, High CO2 permeation flux enabled by highly interconnected three-dimensional ionic channels in selective CO2 separation membranes, Energy Environ. Sci. 5 (2012) 8310.
- [21] N. Xu, X. Li, M.A. Franks, H. Zhao, K. Huang, Silver-molten carbonate composite as a new high-flux membrane for electrochemical separation of CO2 from flue gas, J. Membr. Sci. 401–402 (2012) 190–194.

- [22] S. Wang, J. Tong, L. Cui, P. Zhang, F. Zhou, A layered perovskite La1· 5Sr0· 5NiO4 ±δ-molten carbonate dual-phase membrane for CO2 capture from simulated flue gas, J. Membr. Sci. 647 (2022), 120278.
- [23] O. Ovalle-Encinia, H.-C. Wu, T. Chen, J.Y. Lin, CO2-permselective membrane reactor for steam reforming of methane, J. Membr. Sci. 641 (2022), 119914.
- [24] S.G. Carvalho, E.N. Muccillo, F.C. Fonseca, M. Müller, F. Schulze-Küppers, S. Baumann, W.A. Meulenberg, O. Guillon, R. Muccillo, Tape-casting and freezedrying gadolinia-doped ceria composite membranes for carbon dioxide permeation, J. Membr. Sci. 648 (2022), 120355.
- [25] L.M. Robeson, The upper bound revisited, J. Membr. Sci. 320 (2008) 390-400.
- [26] M.M. Dal-Cin, A. Kumar, L. Layton, Revisiting the experimental and theoretical upper bounds of light pure gas selectivity-permeability for polymeric membranes, J. Membr. Sci. 323 (2008) 299–308.
- [27] P. Zhang, J. Tong, K. Huang, A self-forming dual-phase membrane for high-temperature electrochemical CO2 capture, J. Mater. Chem. 5 (2017) 12769–12773.
- [28] P. Zhang, J. Tong, K. Huang, Self-formed, mixed-conducting, triple-phase membrane for efficient CO2/O2 capture from flue gas and in situ dry-oxy methane reforming, ACS Sustain. Chem. Eng. 6 (2018) 14162–14169.
- [29] Z. Xu, Q. Zheng, S. Wang, Z. Zhang, Z. Liu, G. Zhang, W. Jin, Fabrication of molten nitrate/nitrite dual-phase four-channel hollow fiber membranes for nitrogen oxides separation, J. Membr. Sci. 635 (2021), 119506.
- [30] T. Chen, Y. Xu, Y. Zhang, Y. Gong, Y. Zhang, J.Y. Lin, Double-layer ceramic-carbonate hollow fiber membrane with superior mechanical strength for CO2 separation, J. Membr. Sci. (2022), 120701.
- [31] H.-C. Wu, Z. Rui, J.Y. Lin, Hydrogen production with carbon dioxide capture by dual-phase ceramic-carbonate membrane reactor via steam reforming of methane, J. Membr. Sci. 598 (2020), 117780.
- [32] X. Dong, Y. Lin, Catalyst-free ceramic-carbonate dual phase membrane reactor for hydrogen production from gasifier syngas, J. Membr. Sci. 520 (2016) 907–913.
- [33] O. Ovalle-Encinia, J.Y. Lin, High-pressure CO2 permeation properties and stability of ceramic-carbonate dual-phase membranes, J. Membr. Sci. 646 (2022), 120249.
- [34] Y. Lin, A. Burggraaf, Experimental studies on pore size change of porous ceramic membranes after modification, J. Membr. Sci. 79 (1993) 65–82.
- [35] K. Zhang, S. Sun, N. Xu, K. Huang, H2O-enhanced CO2 transport through a proton conducting ceramic-molten carbonate dual-phase membrane, J. Membr. Sci. 650 (2022), 120421.
- [36] L. Zhang, N. Xu, X. Li, S. Wang, K. Huang, W.H. Harris, W.K. Chiu, High CO 2 permeation flux enabled by highly interconnected three-dimensional ionic channels in selective CO 2 separation membranes, Energy Environ. Sci. 5 (2012) 8310–8317.
- [37] S. Sun, Y. Wen, K.J.A.S.C. Huang, Engineering, A new ceramic-carbonate dualphase membrane for high-flux, CO2 Capture 9 (2021) 5454–5460.
- [38] M. Zuo, S. Zhuang, X. Tan, B. Meng, N. Yang, S. Liu, Ionic conducting ceramic-carbonate dual phase hollow fibre membranes for high temperature carbon dioxide separation, J. Membr. Sci. 458 (2014) 58–65.
- [39] S. Zhuang, Y. Li, M. Zuo, X. Tan, B. Meng, N. Yang, S. Liu, Dense composite electrolyte hollow fibre membranes for high temperature CO2 separation, Separ. Purif. Technol. 132 (2014) 712–718.
- [40] X. Jiang, J. Zhu, Z. Liu, S. Guo, W. Jin, CO2-tolerant SrFe0. 8Nb0. 2O3 δ-carbonate dual-phase multichannel hollow fiber membrane for CO2 capture, Ind. Eng. Chem. Res. 55 (2016) 3300–3307.
- [41] T. Chen, Z. Wang, J. Hu, M.H. Wai, S. Kawi, Y. Lin, High CO2 permeability of ceramic-carbonate dual-phase hollow fiber membrane at medium-high temperature, J. Membr. Sci. 597 (2020), 117770.